On the Internal Semantics of Time-Series Foundation Models

Atharva Pandey[*]
Kairosity
atpan@kairosity.ai

Abhilash Neog[*]
Virginia Tech
abhilash22@vt.edu

Gautam Jajoo
Kairosity
jajoo@kairosity.ai

Abstract

Time-series Foundation Models (TSFMs) have recently emerged as a universal paradigm for learning across diverse temporal domains. However, despite their empirical success, the internal mechanisms by which these models represent fundamental time-series concepts remain poorly understood. In this work, we undertake a systematic investigation of concept interpretability in TSFMs. Specifically, we examine: (i) which layers encode which concepts, (ii) whether concept parameters are linearly recoverable, (iii) how representations evolve in terms of concept disentanglement and abstraction across model depth, and (iv) how models process compositions of concepts. We systematically probe these questions using layer-wise analyses, linear recoverability tests, and representation similarity measures, providing a structured account of TSFM semantics. The resulting insights show that early layers mainly capture local, time-domain patterns (e.g., AR(1), level shifts, trends), while deeper layers encode dispersion and change-time signals, with spectral and warping factors remaining the hardest to recover linearly. In compositional settings, however, probe performance degrades, revealing interference between concepts. This highlights that while atomic concepts are reliably localized, composition remains a challenge, underscoring a key limitation in current TSFMs' ability to represent interacting temporal phenomena.

1 Introduction

Foundation models have recently been extended to time series, where large-scale pretraining over heterogeneous temporal data yields strong zero/few-shot performance in forecasting and classification across healthcare, finance, climate, and energy [Das et al., 2023, Ansari et al., 2024, Goswami et al., 2024, Woo et al., 2024, Garza et al., 2023]. Yet, unlike language and vision, our understanding of what these models encode internally remains limited. Interpretability in NLP and CV has shown that probing methods like linear and structural probes as well as representational similarity can localize information across layers and provide insight into model organization [Alain and Bengio, 2016, Hewitt and Manning, 2019, Kornblith et al., 2019]. For TSFMs, early studies such as [Wiliński et al., 2024] reveal block-like layer similarity and the success of latent interventions, underscoring the value of probing. Complementary instance-level explanations in time series, e.g., saliency, attribution, and shapelets, offer rationales for individual predictions but do not illuminate model-wide semantics [Ismail et al., 2020, Grabocka et al., 2014].

This gap motivates a systematic investigation into how TSFMs internally represent fundamental time-series phenomena. We study *concept interpretability* in TSFMs across seven canonical concepts that span stochastic, structural, and spectral behavior: *AR1*, *Level Shift*, *Random Walk*, *Spectral*, *Time Warped*, *Trend*, and *Variance Shift*. Our analysis is guided by four central questions: **RQ1** - Where do concepts localize across layers? **RQ2** - Are concept parameters linearly recoverable from

[*]Equal contribution.

NeurIPS 2025 Workshop on Recent Advances in Time Series Foundation Models (BERT^{2}S).

intermediate embeddings? **RQ3** - How do representations evolve in terms of disentanglement and abstraction with depth? and **RQ4** - How do models represent compositions of concepts?

To address these questions, we employ a probing-based interpretability framework. Methodologically, we adapt established tools - linear probes, structural probes, and CKA - tailored to quantify concept presence and parameter recoverability [Alain and Bengio, 2016, Hewitt and Manning, 2019, Kornblith et al., 2019]. While these diagnostics are widely used in other domains, their systematic application to a controlled, diverse suite of time-series concepts offers new insights into the inductive biases and limitations of modern TSFMs [Das et al., 2023, Ansari et al., 2024, Goswami et al., 2024, Woo et al., 2024, Garza et al., 2023, Wiliński et al., 2024].

Contributions. (i) A *concept-centric probing framework* for TSFMs covering seven canonical time-series concepts; (ii) *diagnostic tasks* for assessing concept localization, parameter recoverability, and compositional interaction; (iii) *empirical insights* revealing inductive biases and failure modes, which may potentially inform architectural choices, training curricula, and evaluation protocols.

2 Methods

Layer-wise Concept Probing. *RQ1* and *RQ2* examine which concepts are encoded across layers and whether their parameters are linearly recoverable. We investigate this by analyzing the latent representations of each layer using linear probes - a methodology widely used in language models to reveal the emergence of syntax and semantics at specific depths. For time series, this allows us to pinpoint where autoregressive structure, spectral frequency, or trend parameters become accessible. Given a synthetic dataset $\mathbf{X} \in \mathbb{R}^{S \times V}$ with generative parameters θ (e.g., AR coefficient, trend slope, frequency amplitude), a TSFM with L layers produces hidden states $\mathbf{H}^{(l)} = f^{(l)}(\mathbf{X}) \in \mathbb{R}^{S \times d}$, which are pooled into $\mathbf{z}^{(l)} = \text{Pool}(\mathbf{H}^{(l)}) \in \mathbb{R}^d$. A linear probe then predicts parameters as $\hat{\theta}^{(l)} = \mathbf{W}^{(l)}\mathbf{z}^{(l)} + \mathbf{b}^{(l)}$. Performance is measured by mean squared error, $\mathcal{L}^{(l)} = \frac{1}{N}\sum_{i=1}^{N} \|\theta_i - \hat{\theta}_i^{(l)}\|^2$, quantifying parameter recoverability across depth.

Concept Representation. *RQ3* examines how representations evolve across depth - whether they become more abstract or more disentangled. In computer vision, representational similarity analyses reveal progressive shifts from low-level edges to object-level semantics. We adopt a similar lens for TSFMs, asking whether distinct time-series concepts occupy separable or overlapping regions in embedding space, and how this organization changes across layers. To quantify representational similarity across concepts and layers, we compute centered kernel alignment (CKA) between embedding sets $\mathbf{H}^{(l_1)}$ and $\mathbf{H}^{(l_2)}$: $\text{CKA}(\mathbf{H}^{(l_1)}, \mathbf{H}^{(l_2)}) = \frac{\|\mathbf{H}^{(l_1)\top}\mathbf{H}^{(l_2)}\|_F^2}{\|\mathbf{H}^{(l_1)\top}\mathbf{H}^{(l_1)}\|_F \, \|\mathbf{H}^{(l_2)\top}\mathbf{H}^{(l_2)}\|_F}$. Additionally, we visualize embeddings via PCA, UMAP, and t-SNE [Jolliffe, 2002, McInnes et al., 2018, van der Maaten and Hinton, 2008] applied to pooled vectors $\mathbf{z}^{(l)}$, allowing inspection of cluster structure and concept separation.

Concept Composition. *RQ4* examines how TSFMs handle compositions and whether concept-specific information transfers to their mixtures. We adopt a two-step *probe-transfer* protocol: (i) train layer-wise linear probes on *atomic* data for each concept C_j to predict its parameters θ_j (backbone frozen); (ii) evaluate these frozen probes for C_1 and C_2 on *composite* series to assess whether the original parameters remain linearly recoverable. We report per-layer MSE on composite data.

We study two families of compositions: *structured* (segment-wise interleaving with continuity preservation) and *functional* (additive mixing, optionally with per-series normalization and mixing coefficients α). Full construction details, masks, and sampling ranges are provided in Appendix D.

3 Results and Discussions

RQ1 & RQ2*: *Which layers encode which concepts, and are parameters linearly recoverable?

UMAP-probe alignment. Examining UMAP embeddings of layer-wise latent representations reveals how the model organizes conceptual information internally. When representations are compact and well-ordered, linear probes can recover concept parameters with low error, suggesting the model forms localized embeddings for those concepts. Further, when a parameter varies smoothly along the UMAP manifold, probe accuracy improves even more - indicating that the model has not only captured the concept but also encoded a meaningful, controllable parameterization. Such alignment could be

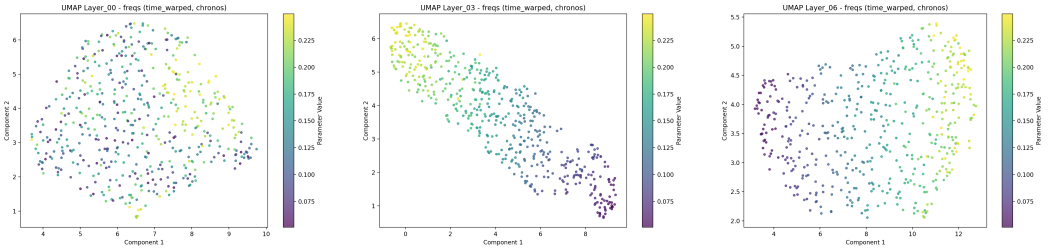

Figure 1: UMAP of pooled embeddings at early, mid, and late layers, time-warp concept.

particularly useful for applications that steer activations conditionally. Through our experiments, we observe that structural and time-domain concepts such as AR(1) coefficient, trend slope, and level shifts, tend to be well-captured with lower probe errors. In contrast, spectral and time-warping concepts exhibit fragmented or tangled UMAP structures and higher probe errors, reflecting non-linear entanglement that resists simple linear decoding (see Fig.1 and AppendixG).

Model comparison and depth. Across identical experimental setups, CHRONOS consistently produces better-organized UMAP representations that are more linearly recoverable than those of MOMENT for all evaluated concepts. Most concepts are captured early-typically by the second transformer layer-after which performance plateaus. In contrast, representations of dispersion and change-point phenomena (e.g., variance shifts) continue to improve with depth, becoming more localized in the later layers (Fig. 1).

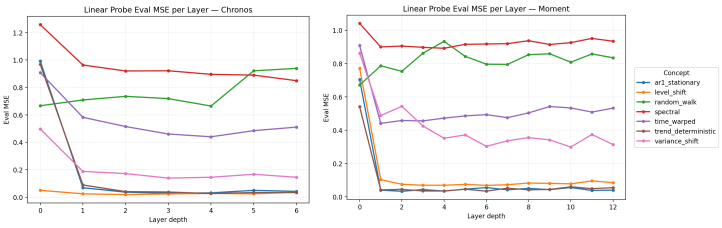

Figure 2: Layer-wise probe (y-axis MSE; x-axis layers) for Chronos (left) and MOMENT (right). Each curve represents a concept

Simple structural and time-domain concepts emerge early in well-organized, linearly recoverable representations, while complex or change-sensitive patterns gradually refine in deeper layers, reflecting a layered hierarchy of concept learning.

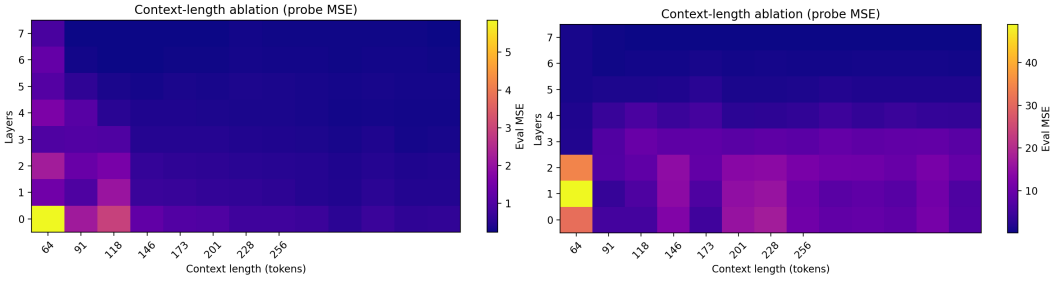

(a) Time Warped Concept (b) Variance Shift Concept

Figure 3: Context Length ablations on MOMENT

RQ3: How do representations evolve with depth?

UMAP snapshots (see Figures in the Appendix G, for e.g. Figure 13 and Figure 14) reveal increasing cluster separation from early to late layers. *Early layers reflect locally volatile structure; mid layers show partial disentanglement; late layers consolidate concept-level separation while compressing intra-concept variance.* This pattern aligns with the drop in probe MSE after layer 1, indicating a shift from generic to concept-aligned features.

We further probe each layer's reliance on temporal context by cropping inputs to multiple fractions (25-100%), extracting pooled embeddings, and evaluating the pretrained per-layer linear probes on the target concept. From Figure 49a and Figure 49b we can see how MSE changes with available history; *deeper layers improve as context grows (encoding longer-range dynamics) compared to relatively less improvement in early layers (capturing short, local structure).*

RQ4: How are concept compositions represented?

TSFMs can effectively encode atomic time-series concepts, but real-world data often involves compositions of multiple concepts. To study the behavior of TSFMs under composite concepts, we conduct two complementary experiments: **(a) Vector Arithmetic** - Inspired by word embedding compositionality, we test whether TSFM embeddings exhibit similar additive properties. Specifically, we evaluate whether the element-wise sum of atomic concept embeddings ($\mathbf{emb_1} + \mathbf{emb_2}$) approximates the embedding of their composite concept ($\mathbf{emb_3}$) using cosine similarity and relative distance metrics across model layers. **(b) Temporal Alignment Analysis** - Since time-series have inherent temporal structure, we test compositional stability across different sequence lengths (32, 64, 128, 256 timesteps). This assesses whether compositional relationships hold consistently across temporal horizons or are sensitive to sequence length.

Figure 4 **reveals** strong compositional properties in TSFMs, with cosine similarities approaching 1.0 across most layers, indicating that atomic concept embeddings combine nearly linearly ($\mathbf{emb_1} + \mathbf{emb_2} \approx \mathbf{emb_3}$). Performance degradation in initial and final layers suggests that early representations lack full compositional structure, while deeper layers specialize in task-specific features that deviate from additive composition. The anomalous behavior of *spectral+level shift*, which shows substantially higher relative distances, indicates non-linear interactions between concepts with fundamentally different temporal characteristics-frequency-domain properties versus abrupt discontinuities. *Overall, TSFMs learn compositional representations similar to word embeddings for most concept pairs, with notable exceptions requiring more sophisticated composition mechanisms for temporally disparate concepts.*

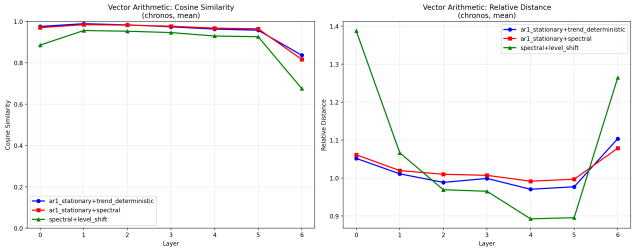

Figure 4: Vector arithmetic experiments with CHRONOS. Atomic embeddings combine nearly linearly ($\mathbf{emb_1} + \mathbf{emb_2} \approx \mathbf{emb_3}$), except for temporally disparate concept pairs.

The temporal alignment analysis results (see Figure 5) **demonstrate** robust compositional stability across sequence lengths, with consistently high similarities throughout most layers and temporal horizons. Reduced similarity at shorter sequences (32–128) in the initial and final layers suggests that compositional understanding requires sufficient temporal context to emerge and stabilize. *The uniformly high performance at longer sequences confirms that TSFMs' compositional properties are temporally robust once adequate context is provided.* Please refer to Appendix H for add. results.

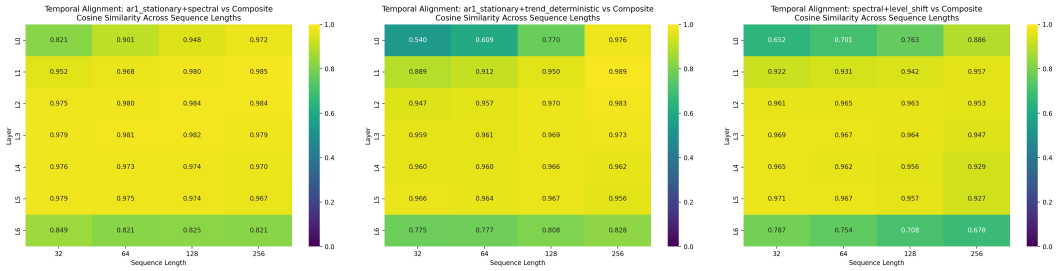

Figure 5: Chronos – Temporal alignment experiments. We show stability of compositional relationships across multiple atomic-concept pairs.

4 Conclusion and Future Work

We present a probe-based analysis of time-series foundation models across seven canonical concepts. Early layers expose local, time domain structure (AR(1), level shift, trend), deeper layers specialize in dispersion and change-point signals. Spectral and time-warping factors are the least linearly accessible. TSFMs also exhibit strong linear compositional properties across most layers and concept pairs. Future works could explore additional TSFMs, multivariate and irregular datasets; adopt controlled-capacity non-linear or causal probes; architectures and objectives that better linearize phase and time-warping, and non-linear conditional steering.

References

Guillaume Alain and Yoshua Bengio. Understanding intermediate layers using linear classifier probes. *arXiv preprint arXiv:1610.01644*, 2016. doi: 10.48550/arXiv.1610.01644. URL https://arxiv.org/abs/1610.01644.

Abdul Fatir Ansari, Lorenzo Stella, Caner Turkmen, Xiyuan Zhang, Pedro Mercado, Huibin Shen, Oleksandr Shchur, Syama Sundar Rangapuram, Sebastian Pineda Arango, Shubham Kapoor, Jasper Zschiegner, Danielle C. Maddix, Hao Wang, Michael W. Mahoney, Kari Torkkola, Andrew Gordon Wilson, Michael Bohlke-Schneider, and Yuyang Wang. Chronos: Learning the language of time series. *arXiv preprint arXiv:2403.07815*, 2024. doi: 10.48550/arXiv.2403.07815. URL https://arxiv.org/abs/2403.07815.

Abhimanyu Das, Weihao Kong, Rajat Sen, and Yichen Zhou. A decoder-only foundation model for time-series forecasting. *arXiv preprint arXiv:2310.10688*, 2023. doi: 10.48550/arXiv.2310.10688. URL https://arxiv.org/abs/2310.10688.

Azul Garza, Cristian Challu, and Max Mergenthaler-Canseco. Timegpt-1. *arXiv preprint arXiv:2310.03589*, 2023. doi: 10.48550/arXiv.2310.03589. URL https://arxiv.org/abs/2310.03589.

Mononito Goswami, Konrad Szafer, Arjun Choudhry, Yifu Cai, Shuo Li, and Artur Dubrawski. MOMENT: A family of open time-series foundation models. In *Proceedings of the 41st International Conference on Machine Learning*, volume 235 of *Proceedings of Machine Learning Research*, pages 16115–16152. PMLR, 2024. URL https://proceedings.mlr.press/v235/goswami24a.html.

Josif Grabocka, Nicolas Schilling, Martin Wistuba, and Lars Schmidt-Thieme. Learning time-series shapelets. In *Proceedings of the 20th ACM SIGKDD International Conference on Knowledge Discovery and Data Mining*, pages 392–401. ACM, 2014. doi: 10.1145/2623330.2623613. URL https://dl.acm.org/doi/10.1145/2623330.2623613.

John Hewitt and Christopher D. Manning. A structural probe for finding syntax in word representations. In *Proceedings of the 2019 Conference of the North American Chapter of the Association for Computational Linguistics: Human Language Technologies*, pages 4129–4138, Minneapolis, Minnesota, 2019. Association for Computational Linguistics. doi: 10.18653/v1/N19-1419. URL https://aclanthology.org/N19-1419/.

Aya Abdelsalam Ismail, Mohamed Gunady, Héctor Corrada Bravo, and Soheil Feizi. Benchmarking deep learning interpretability in time series predictions. In *Advances in Neural Information Processing Systems*, volume 33, pages 6441–6452, 2020. URL https://proceedings.neurips.cc/paper/2020/file/47a3893cc405396a5c30d91320572d6d-Paper.pdf.

Ian T. Jolliffe. *Principal Component Analysis*. Springer, New York, NY, second edition, 2002. doi: 10.1007/b98835.

Simon Kornblith, Mohammad Norouzi, Honglak Lee, and Geoffrey Hinton. Similarity of neural network representations revisited. In *Proceedings of the 36th International Conference on Machine Learning*, volume 97 of *Proceedings of Machine Learning Research*, pages 3519–3529. PMLR, 2019. URL https://proceedings.mlr.press/v97/kornblith19a.html.

Leland McInnes, John Healy, and James Melville. Umap: Uniform manifold approximation and projection for dimension reduction. *arXiv preprint arXiv:1802.03426*, 2018. URL https://arxiv.org/abs/1802.03426.

Laurens van der Maaten and Geoffrey Hinton. Visualizing data using t-sne. *Journal of Machine Learning Research*, 9:2579–2605, 2008. URL https://www.jmlr.org/papers/v9/vandermaaten08a.html.

Michał Wiliński, Mononito Goswami, Nina Żukowska, Willa Potosnak, and Artur Dubrawski. Exploring representations and interventions in time series foundation models. *arXiv preprint arXiv:2409.12915*, 2024. URL https://arxiv.org/abs/2409.12915.

Gerald Woo, Chenghao Liu, Akshat Kumar, Caiming Xiong, Silvio Savarese, and Doyen Sahoo. Unified training of universal time series forecasting transformers. In *Proceedings of the 41st International Conference on Machine Learning*, volume 235 of *Proceedings of Machine Learning Research*, pages 53140–53164. PMLR, 2024. URL https://proceedings.mlr.press/v235/woo24a.html.

A Related Works

Time-series foundation models. Recent TSFMs demonstrate strong zero/few-shot performance via large-scale pretraining and task-agnostic architectures. Representative families include TimesFM (decoder-only with patched attention), Chronos (tokenized values with T5-style training), MOMENT (open models and the Time Series Pile), Moirai (masked-encoder universal forecaster), and TimeGPT (closed-source API). These works establish the empirical promise of TSFMs but do not characterize concept-level internal semantics. [Das et al., 2023, Ansari et al., 2024, Goswami et al., 2024, Woo et al., 2024, Garza et al., 2023]

Probing and representational similarity. Linear probes and related diagnostic tools are widely used to localize information across layers in deep networks, originating with linear classifier probes and extended by structural probes in NLP to test linear recoverability of syntax. Centered Kernel Alignment (CKA) is commonly used to compare layer representations within and across models due to its invariances and robustness relative to earlier CCA-style measures. Our study adapts these established tools to TSFMs and focuses them on time-series concepts and parameters. [Alain and Bengio, 2016, Hewitt and Manning, 2019, Kornblith et al., 2019]

Interpreting TSFMs and time-series models. Closest to our work, Wiliński et al. analyze internal redundancy and concept steering in TSFMs, reporting block-like layer similarity and latent-space interventions; we complement this by centering *concept parameters*, layer-wise recoverability, and controlled compositions. Broader interpretability for time series has emphasized saliency/attribution and shapelet-based explanations; these provide instance-level rationales, whereas our focus is on *representation-level* concept encoding across depth. [Wiliński et al., 2024, Ismail et al., 2020, Grabocka et al., 2014]

B Experimental Setup

Datasets. We evaluate seven synthetic concepts: AR(1), Level Shift, Random Walk, Spectral (sum of sinusoids), Time-Warped Sinusoid, Deterministic Trend, and Variance Shift. Generation procedures, parameter ranges, and normalization rules follow Appendix D (Dataset Generation and Description). We additionally construct compositional datasets by pairing two base concepts.

Models. We use publicly released checkpoints of two time-series foundation models: Chronos and MOMENT since both are T-5 like models transformer architecture. Model weights are frozen and no finetuning is performed.

Evaluation and reporting. We use an 80/20 train/validation split for each concept and composition. Metric is mean squared error (MSE) for parameter recovery.

C Dimensionality Reduction Techniques

Principal Component Analysis (PCA). Given pooled representations $\{\mathbf{z}_i^{(l)}\}_{i=1}^N$, we compute the empirical covariance matrix

$$\mathbf{\Sigma}^{(l)} = \frac{1}{N}\sum_{i=1}^{N}\left(\mathbf{z}_i^{(l)} - \bar{\mathbf{z}}^{(l)}\right)\left(\mathbf{z}_i^{(l)} - \bar{\mathbf{z}}^{(l)}\right)^\top.$$

Eigen-decomposition yields orthogonal axes capturing the largest variance directions:

$$\mathbf{\Sigma}^{(l)}\mathbf{u}_k = \lambda_k \mathbf{u}_k, \quad \lambda_1 \geq \lambda_2 \geq \dots.$$

These principal axes reveal which parameters dominate the representation space and whether layers compress or expand information.

t-SNE. To assess local neighborhoods, we apply t-distributed Stochastic Neighbor Embedding (t-SNE), which constructs pairwise similarities in high- and low-dimensional spaces. For two points $\mathbf{z}_i, \mathbf{z}_j$, their similarity in the original space is

$$p_{ij} = \frac{\exp(-\|\mathbf{z}_i - \mathbf{z}_j\|^2/2\sigma_i^2)}{\sum_{k\neq i}\exp(-\|\mathbf{z}_i - \mathbf{z}_k\|^2/2\sigma_i^2)},$$

while in 2D space the similarity is

$$q_{ij} = \frac{\left(1 + \|\mathbf{y}_i - \mathbf{y}_j\|^2\right)^{-1}}{\sum_{k \neq l} \left(1 + \|\mathbf{y}_k - \mathbf{y}_l\|^2\right)^{-1}}.$$

t-SNE minimizes the Kullback–Leibler divergence:

$$\mathrm{KL}(P\|Q) = \sum_{i \neq j} p_{ij} \log \frac{p_{ij}}{q_{ij}}.$$

This highlights fine-grained clusters and separability of parameter values.

UMAP. Uniform Manifold Approximation and Projection seeks a balance between local and global structure. It constructs a weighted k-nearest-neighbor graph and optimizes a low-dimensional embedding $\{\mathbf{y}_i\}$ by minimizing the cross-entropy between high- and low-dimensional fuzzy simplicial sets:

$$\mathcal{L}_{\text{UMAP}} = \sum_{(i,j)} w_{ij} \log \sigma(\|\mathbf{y}_i - \mathbf{y}_j\|) + (1 - w_{ij}) \log(1 - \sigma(\|\mathbf{y}_i - \mathbf{y}_j\|)),$$

where σ is a differentiable approximation of a step function. UMAP can reveal concept families and hierarchical relationships (e.g., stationary vs. nonstationary).

These projections provide intuition about the embedding geometry—global variance (PCA), local clusters (t-SNE), and local-global trade-offs (UMAP)—which the linear probes then quantify.

D Synthetic Datasets

This section summarizes the synthetic time–series concepts used in our experiments, their generating equations, and key parameters. Unless noted, ε_t denotes i.i.d. Gaussian noise.

D.1 AR(1) (Stationary)

$$x_t = \phi\, x_{t-1} + \varepsilon_t, \quad |\phi| < 1, \tag{1}$$

$$\varepsilon_t \sim \mathcal{N}(0, \sigma^2), \quad x_0 \text{ drawn from the stationary distribution.} \tag{2}$$

Parameters: autoregressive coefficient ϕ (sampled from an interval), innovation std σ. Default normalization: per-series z-score.

D.2 Level Shift

$$x_t = \eta_t + \Delta\, \mathbf{1}\{t \geq \tau\}, \quad \eta_t \sim \mathcal{N}(0, \text{noise\_std}^2). \tag{3}$$

Parameters: signed shift magnitude Δ, changepoint τ, noise std. Default normalization: none (scale encodes the signal).

D.3 Random Walk (With Drift)

$$x_t = x_{t-1} + \mu + \varepsilon_t, \tag{4}$$

$$\varepsilon_t \sim \mathcal{N}(0, \sigma^2). \tag{5}$$

Parameters: drift μ, innovation std. Default normalization: none.

D.4 Spectral (Sum of Sinusoids)

$$x_t = \sum_{j=1}^{k} a_j \sin\left(2\pi f_j t + \phi_j\right) + \varepsilon_t, \quad 0 < f_j < 0.5. \tag{6}$$

Parameters: number of components $k \in \{1, \ldots, k_{\max}\}$; amplitudes a_j; frequencies f_j sampled from [freq_low, freq_high]; phases $\phi_j \sim \text{Uniform}(0, 2\pi)$; noise std. Default normalization: per-series z-score.

D.5 Time-Warped Sinusoid

Generate a base sinusoid $b_t = \sin(2\pi f t + \phi)$, draw positive steps from a Gamma distribution, form a monotone cumulative warp u rescaled to $[0, T-1]$, then reinterpolate back to the regular grid:

$$x_t = \text{interp}(t, u, b) + \varepsilon_t. \tag{7}$$

Parameters: base frequency f, phase ϕ, warp strength, noise std. Default normalization: per-series z-score.

D.6 Deterministic Trend

$$x_t = \beta\, t + \varepsilon_t, \quad \varepsilon_t \sim \mathcal{N}(0, \text{noise\_std}^2). \tag{8}$$

Parameters: slope β, noise std. Default normalization: per-series z-score.

D.7 Variance Shift

$$x_t \sim \begin{cases} \mathcal{N}(0, \sigma_1^2), & t < \tau, \\ \mathcal{N}(0, \sigma_2^2), & t \geq \tau. \end{cases} \tag{9}$$

Parameters: changepoint τ, standard deviations σ_1, σ_2. Default normalization: none.

Notes on Normalization Concepts where magnitude/level is the signal (e.g., level or variance shift, random walk) use no normalization by default; others use per-series z-scoring. See the code reference (`concepts_dataset.py`) for full details and sampling ranges.

D.8 Time-series Concepts

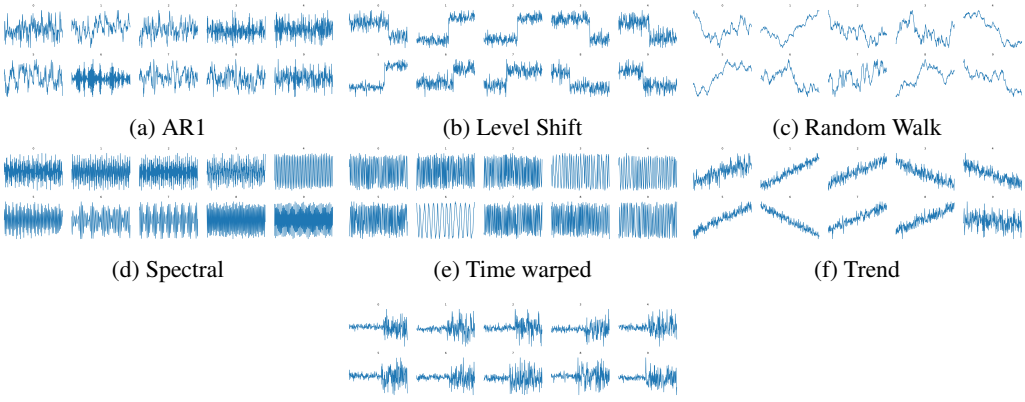

(a) AR1 (b) Level Shift (c) Random Walk

(d) Spectral (e) Time warped (f) Trend

(g) Variance Shift

Figure 6: Visualization of the synthetic time-series samples generated

D.9 Time series composition

Let $\mathcal{T}1 = \{T_1^{(i)}\}i = 1^N$ and $\mathcal{T}2 = \{T_2^{(i)}\}i = 1^N$ be two sets of time series generated from concepts C_1 and C_2 respectively, where each $T_j^{(i)} \in \mathbb{R}^T$.

Structured Composition. Temporal interleaving with continuity constraints, preserving local concept characteristics in different time segments.

For each sample i, we generate breakpoints a_i, b_i where:

$$a_i \sim \mathcal{U}(\lfloor \alpha_{\text{low}} \cdot T \rfloor, \lfloor \alpha_{\text{high}} \cdot T \rfloor)$$

$$b_i \sim \mathcal{U}(\lfloor \beta_{\text{low}} \cdot T \rfloor, \lfloor \beta_{\text{high}} \cdot T \rfloor)$$

with constraints $0 \leq a_i < b_i \leq T$ and default ranges $\alpha_{\text{low}} = 0.2, \alpha_{\text{high}} = 0.4, \beta_{\text{low}} = 0.6, \beta_{\text{high}} = 0.8$. The structured compositional series $X_{\text{struct}}^{(i)}$ is defined as:

$$X_{\text{struct}}^{(i)}[t] = \begin{cases} T_1^{(i)}[t] & \text{if } t < a_i \\ T_2^{(i)}[t] + \delta_1^{(i)} & \text{if } a_i \leq t < b_i \\ T_1^{(i)}[t] + \delta_2^{(i)} & \text{if } t \geq b_i \end{cases}$$

where the continuity offsets are:

$$\delta_1^{(i)} = T_1^{(i)}[a_i] - T_2^{(i)}[a_i]$$

$$\delta_2^{(i)} = T_2^{(i)}[b_i] - T_1^{(i)}[b_i] + \delta_1^{(i)}$$

The corresponding mask $M^{(i)} \in \{0, 1\}^T$ indicates the source concept:

$$M^{(i)}[t] = \begin{cases} 0 & \text{if } t < a_i \text{ or } t > b_i \text{ (from } C_1\text{)} \\ 1 & \text{if } a_i \leq t \leq b_i \text{ (from } C_2\text{)} \end{cases}$$

Functional Composition. Elementwise addition creating global interaction between concepts throughout the entire time series Both approaches generate datasets containing the composed series X, original component series T_1, T_2, and metadata preserving the generative parameters from both source concepts.

For functional composition, we first optionally normalize each time series:

$$\tilde{T}_j^{(i)} = \begin{cases} \frac{T_j^{(i)} - \mu_j^{(i)}}{\sigma_j^{(i)}} & \text{if normalize = True} \\ T_j^{(i)} & \text{otherwise} \end{cases}$$

where $\mu_j^{(i)} = \frac{1}{T} \sum_{t=1}^{T} T_j^{(i)}[t]$ and $\sigma_j^{(i)} = \sqrt{\frac{1}{T} \sum_{t=1}^{T} (T_j^{(i)}[t] - \mu_j^{(i)})^2}$. The functional compositional series is then:

$$X_{\text{func}}^{(i)} = \tilde{T}1^{(i)} + \tilde{T}_2^{(i)}$$

E Layer Representation Similarity

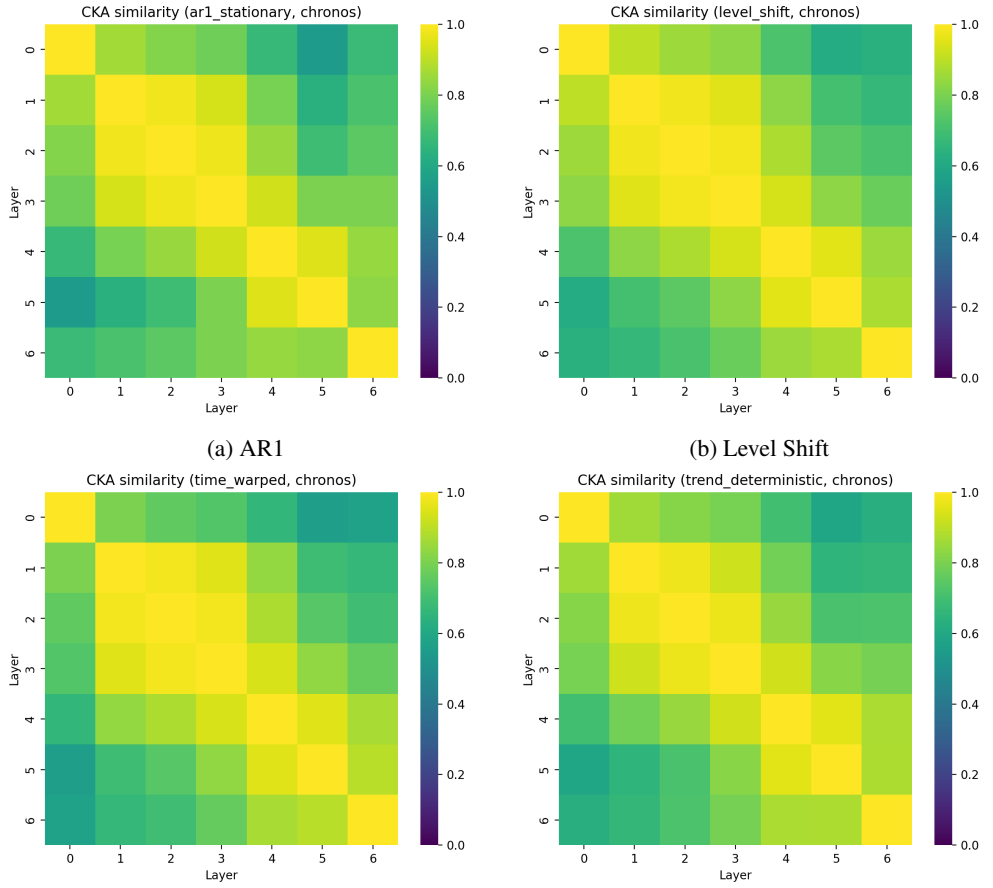

(a) AR1

(b) Level Shift

(c) Time warped

(d) Trend

Figure 7: CKA Similarity among layers of Chronos TSFM

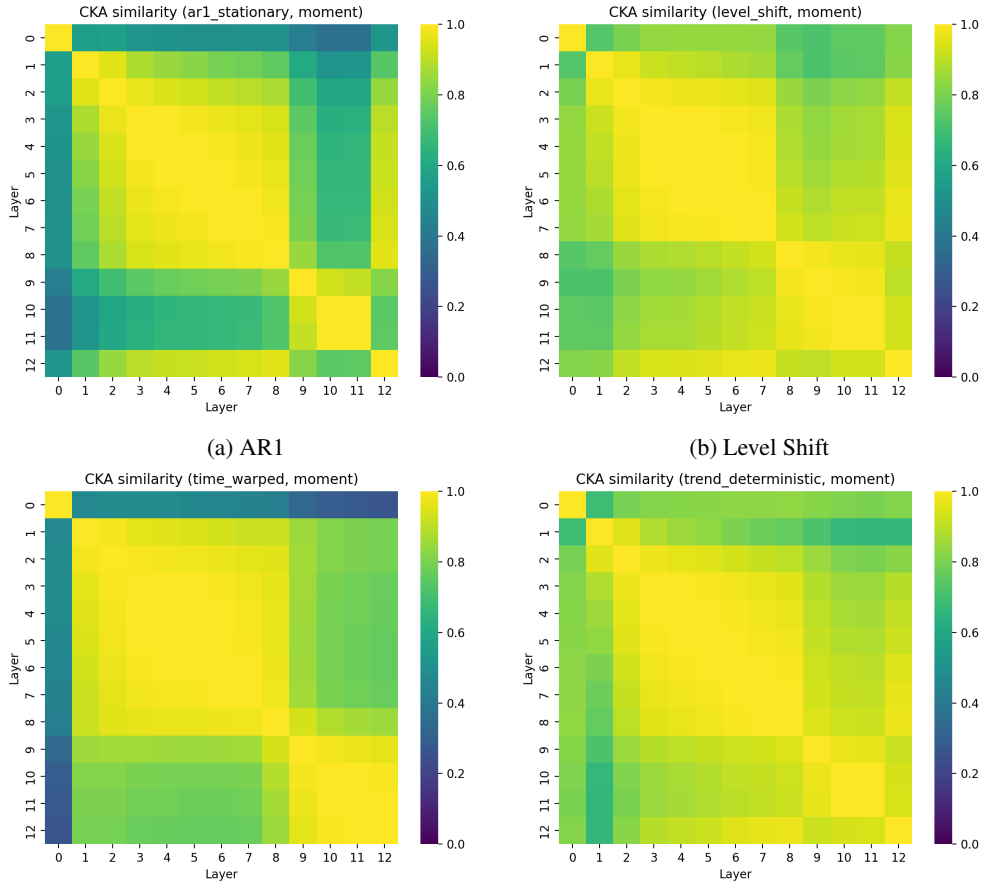

(a) AR1

(b) Level Shift

(c) Time warped

(d) Trend

Figure 8: CKA Similarity among layers of MOMENT TSFM

F Linear Probe Loss

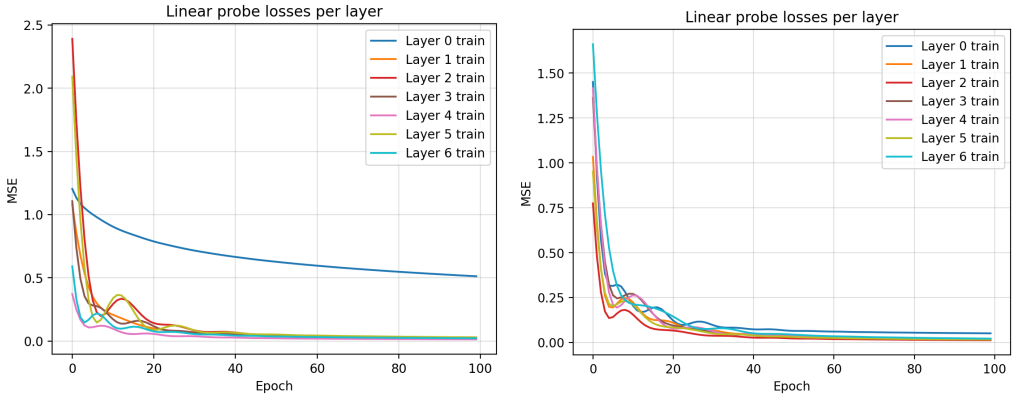

(a) AR1

(b) Level Shift

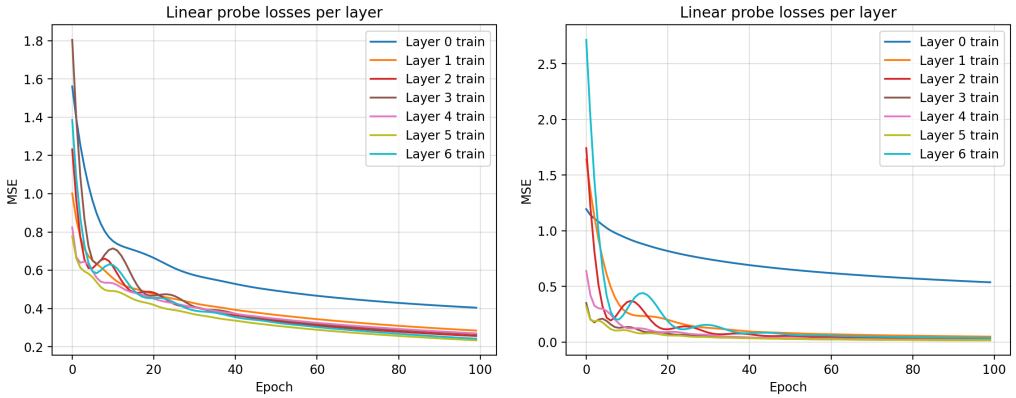

(c) Time warped

(d) Trend

Figure 9: Layer-wise Loss in Chronos TSFM

G Layerwise Respresentation Visualization

This section summarizes layerwise embeddings visualized via PCA, t-SNE, and UMAP for each concept and model. We show triplets of layers per method.

G.1 AR(1) (Stationary)

Moment (parameter: ϕ).

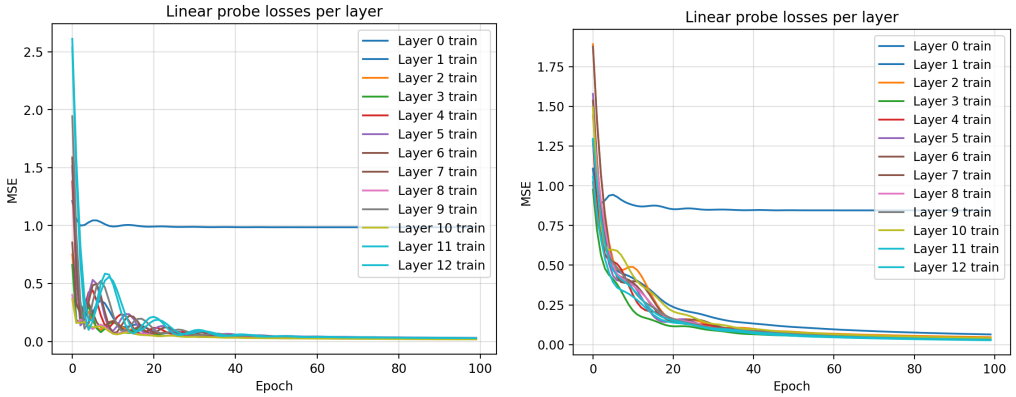

(a) AR1

(b) Level Shift

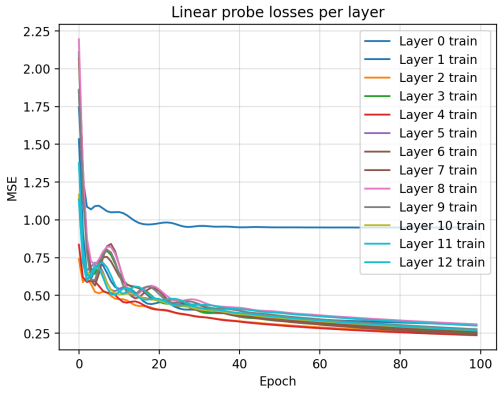

(c) Time warped

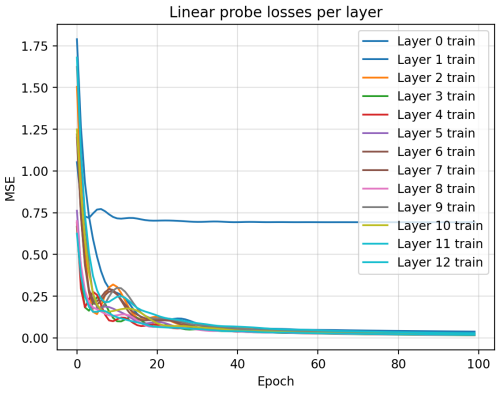

(d) Trend

Figure 10: Layer-wise Loss in MOMENT TSFM

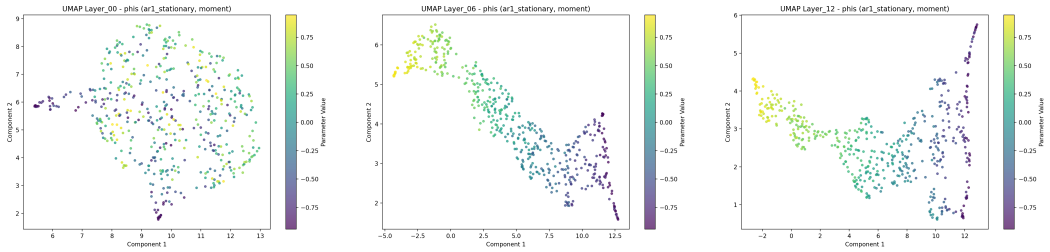

Figure 11: AR(1) — Moment — UMAP (Layers 00/06/12)

Chronos (parameter: ϕ).

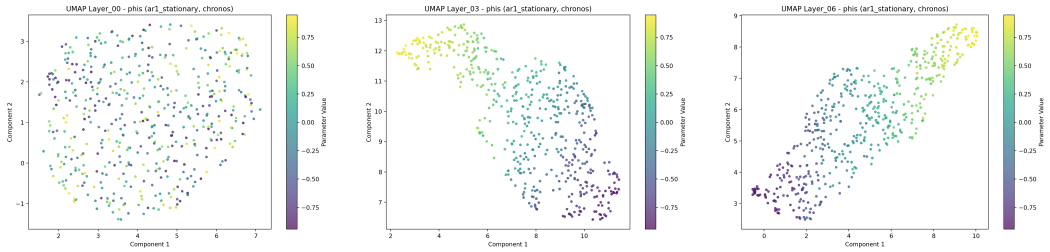

Figure 12: AR(1) — Chronos — UMAP (Layers 00/03/06)

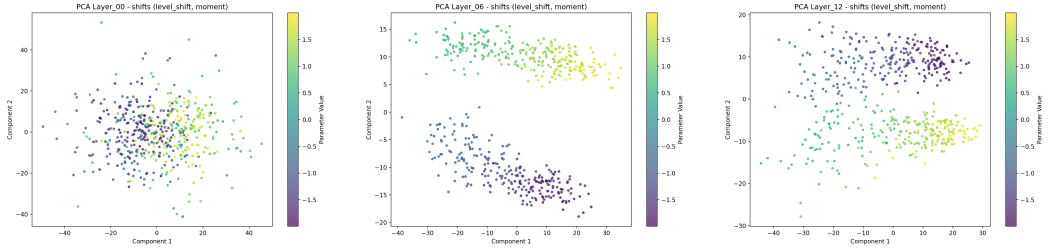

Figure 13: Level Shift — Moment — Shift — PCA (Layers 00/06/12)

G.2 Level Shift

Moment (parameters: shift, τ).

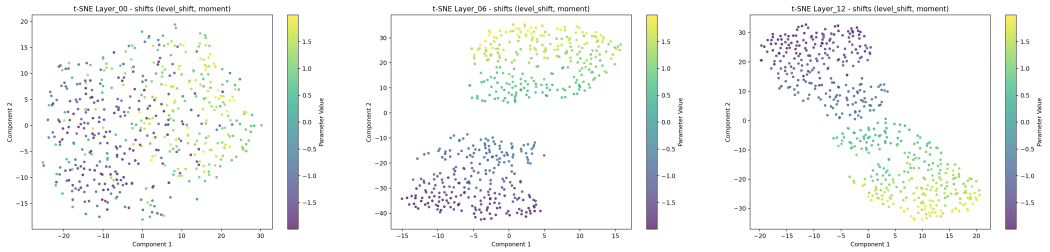

Figure 14: Level Shift — Moment — Shift — t-SNE (Layers 00/06/12)

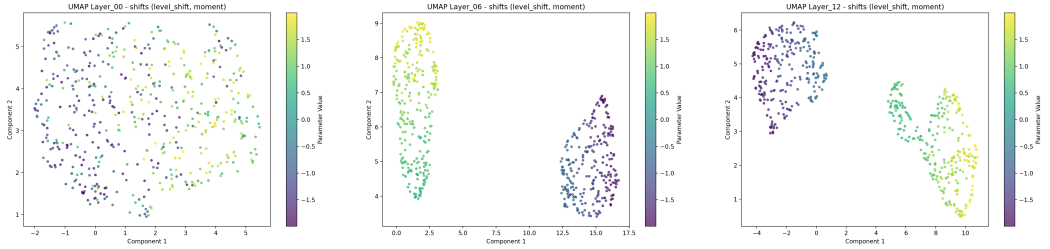

Figure 15: Level Shift — Moment — Shift — UMAP (Layers 00/06/12)

Chronos (parameters: shift, τ).

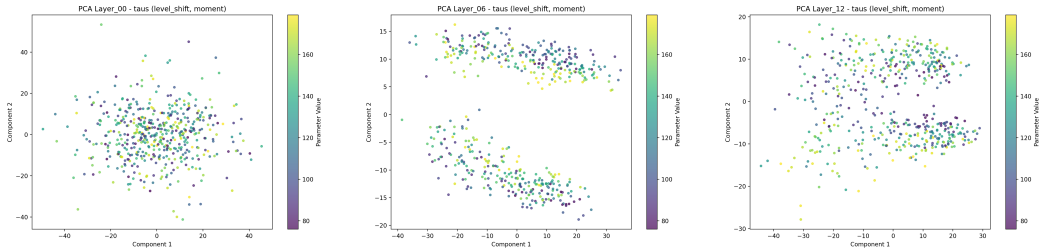

Figure 16: Level Shift — Moment — τ — PCA (Layers 00/06/12)

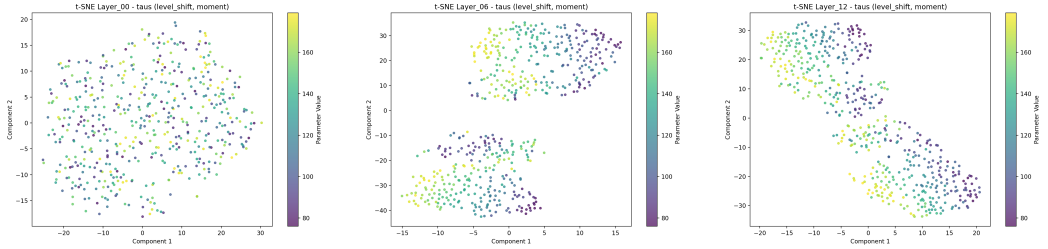

Figure 17: Level Shift — Moment — τ — t-SNE (Layers 00/06/12)

G.3 Random Walk

Chronos (parameter: drift).

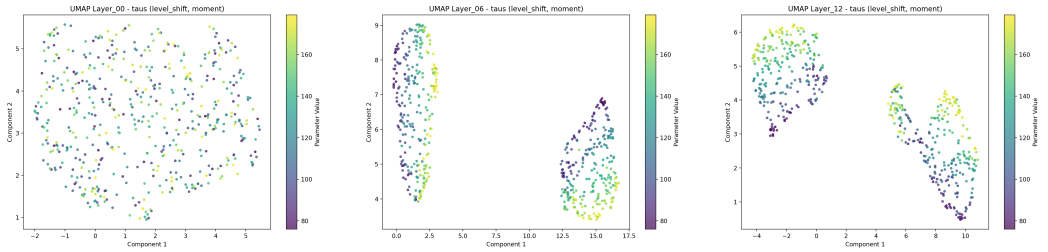

Figure 18: Level Shift — Moment — τ — UMAP (Layers 00/06/12)

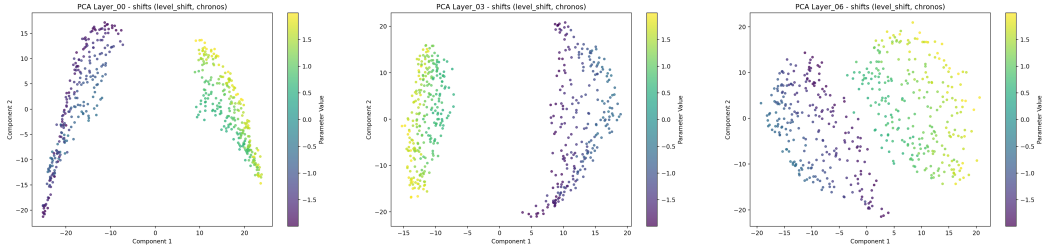

Figure 19: Level Shift — Chronos — Shift — PCA (Layers 00/03/06)

Moment (parameter: drift).

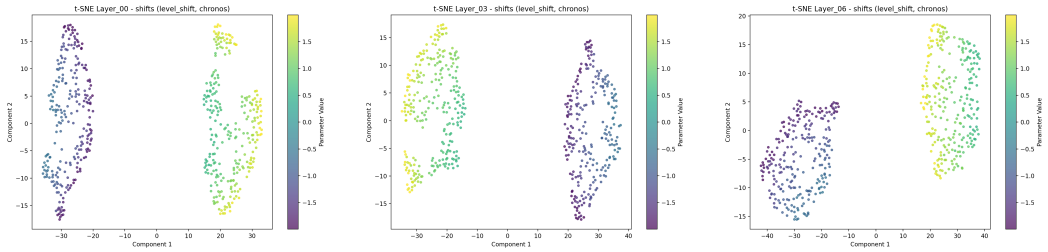

Figure 20: Level Shift — Chronos — Shift — t-SNE (Layers 00/03/06)

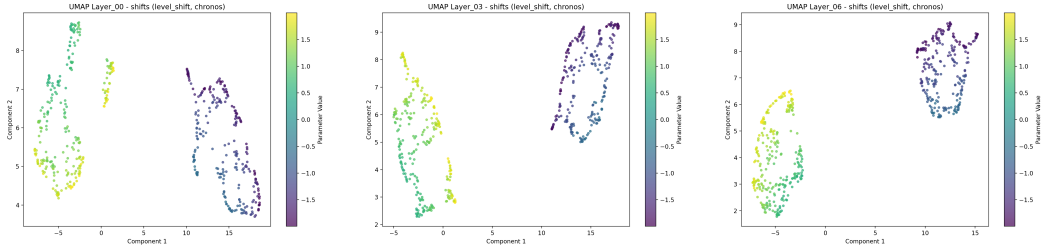

Figure 21: Level Shift — Chronos — Shift — UMAP (Layers 00/03/06)

G.4 Spectral (Sum of Sinusoids)

Chronos (frequency).

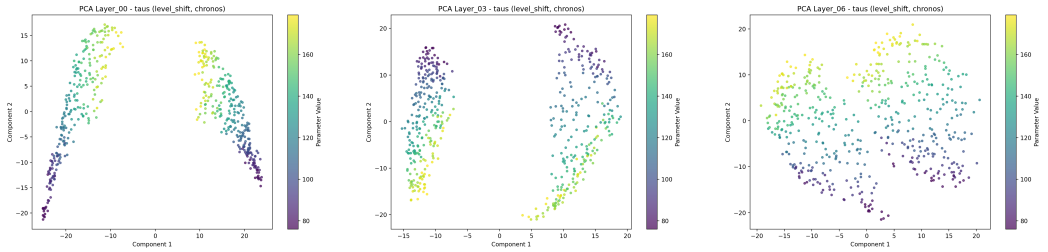

Figure 22: Level Shift — Chronos — τ — PCA (Layers 00/03/06)

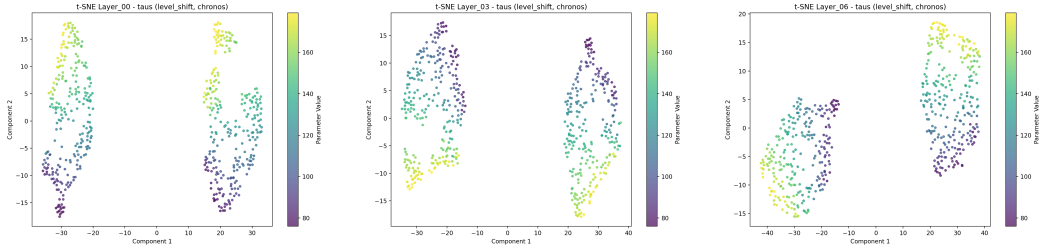

Figure 23: Level Shift — Chronos — τ — t-SNE (Layers 00/03/06)

Moment (frequency).

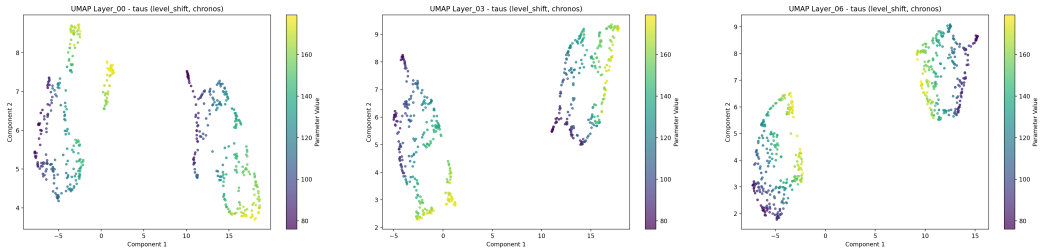

Figure 24: Level Shift — Chronos — τ — UMAP (Layers 00/03/06)

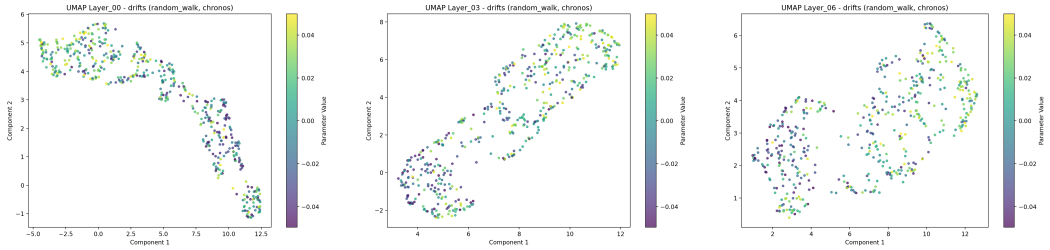

Figure 25: Random Walk — Chronos — UMAP (Layers 00/03/06)

G.5 Time-Warped Sinusoid

Moment (freq).

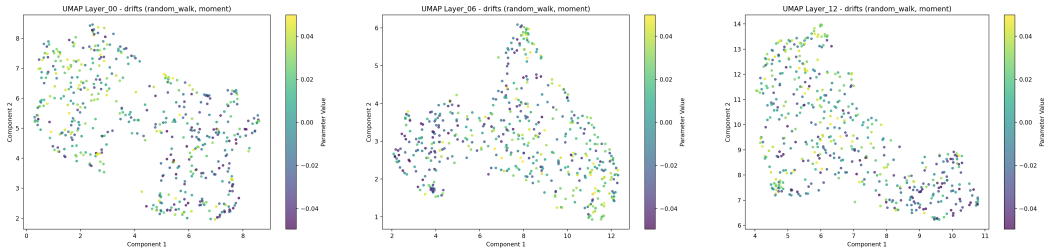

Figure 26: Random Walk — Moment — UMAP (Layers 00/06/12)

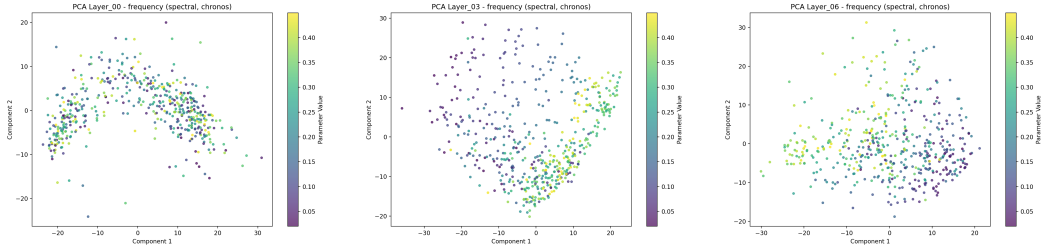

Figure 27: Spectral — Chronos — Frequency — PCA (Layers 00/03/06)

Chronos (freq).

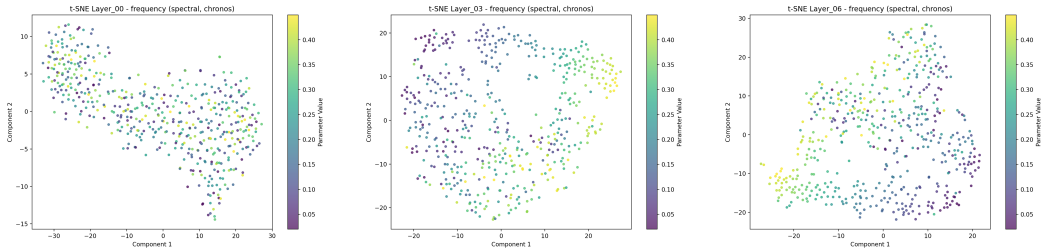

Figure 28: Spectral — Chronos — Frequency — t-SNE (Layers 00/03/06)

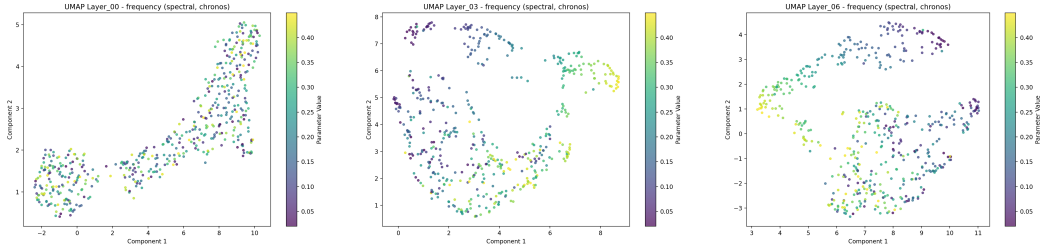

Figure 29: Spectral — Chronos — Frequency — UMAP (Layers 00/03/06)

G.6 Deterministic Trend

Moment (slope).

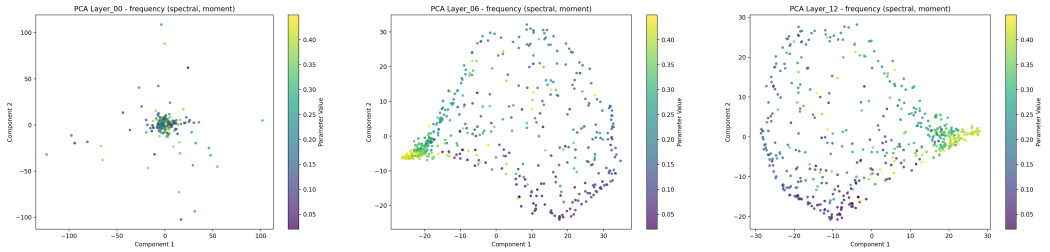

Figure 30: Spectral — Moment — Frequency — PCA (Layers 00/06/12)

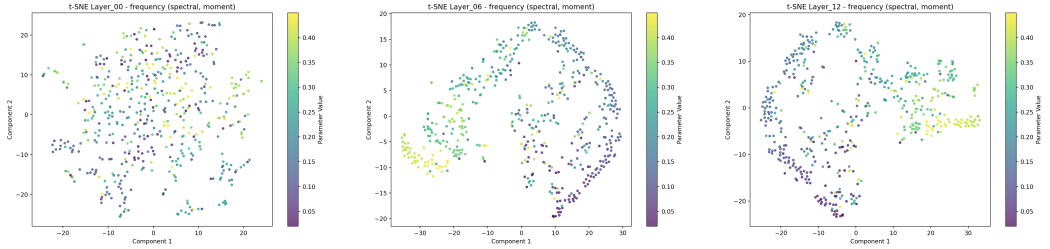

Figure 31: Spectral — Moment — Frequency — t-SNE (Layers 00/06/12)

Chronos (slope).

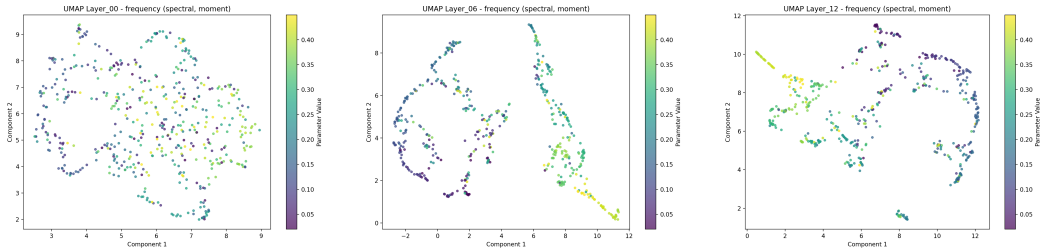

Figure 32: Spectral — Moment — Frequency — UMAP (Layers 00/06/12)

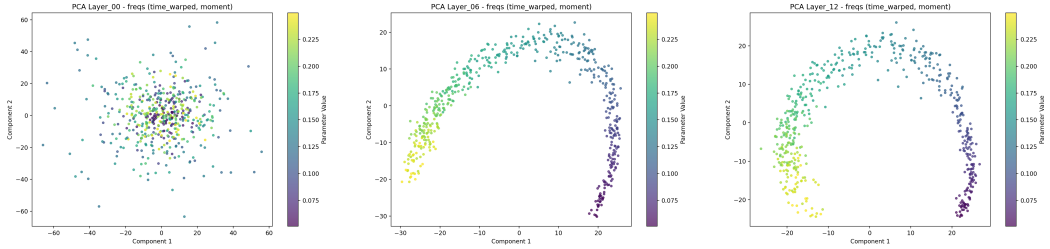

Figure 33: Time-Warped — Moment — Freqs — PCA (Layers 00/06/12)

G.7 Variance Shift

Chronos (τ).

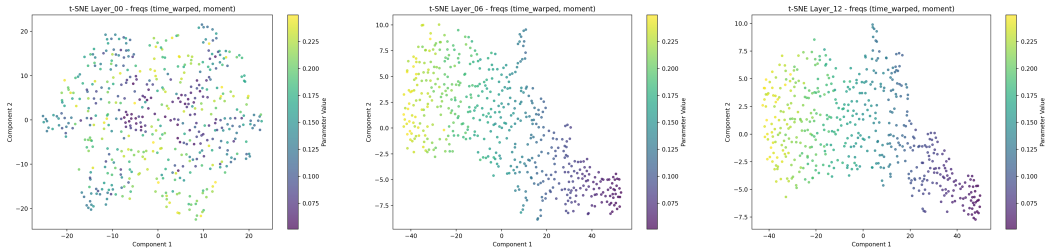

Figure 34: Time-Warped — Moment — Freqs — t-SNE (Layers 00/06/12)

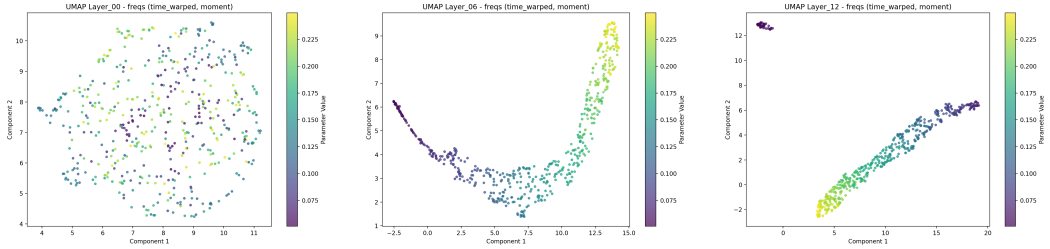

Figure 35: Time-Warped — Moment — Freqs — UMAP (Layers 00/06/12)

Moment (τ).

H Compositionality results

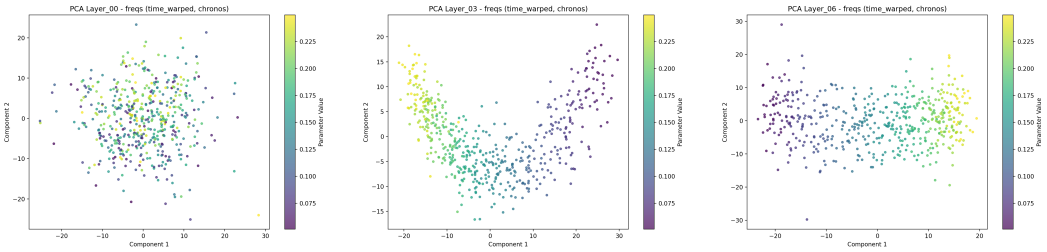

Figure 36: Time-Warped — Chronos — Freqs — PCA (Layers 00/03/06)

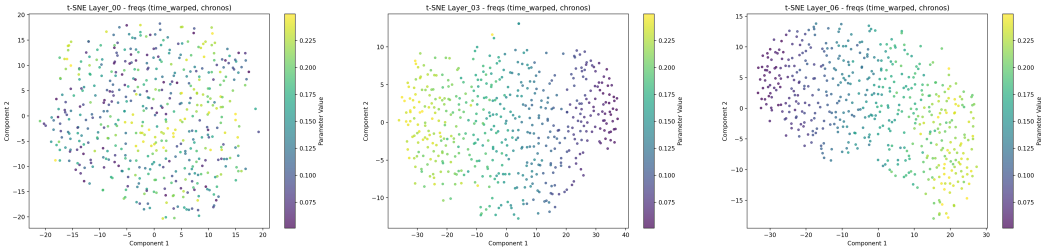

Figure 37: Time-Warped — Chronos — Freqs — t-SNE (Layers 00/03/06)

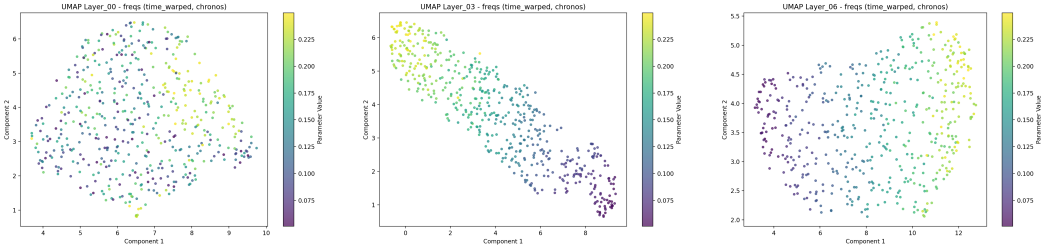

Figure 38: Time-Warped — Chronos — Freqs — UMAP (Layers 00/03/06)

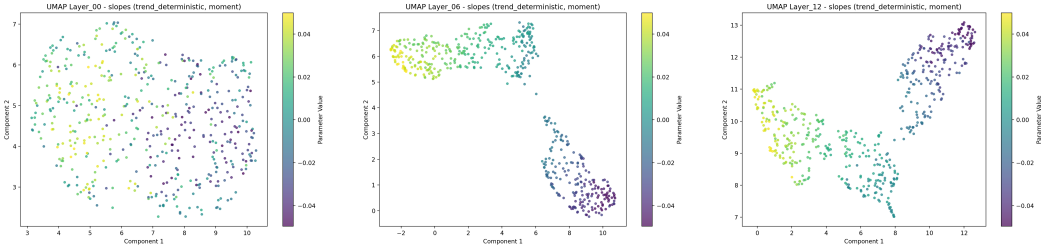

Figure 39: Trend — Moment — UMAP (Layers 00/06/12)

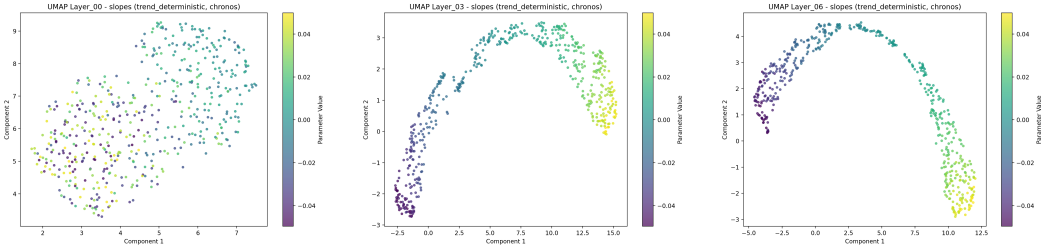

Figure 40: Trend — Chronos — UMAP (Layers 00/03/06)

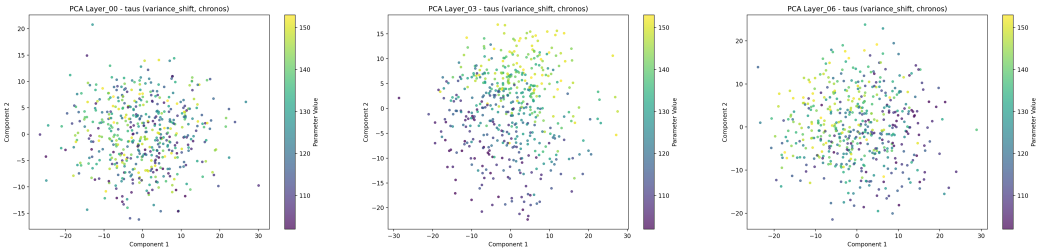

Figure 41: Variance Shift — Chronos — PCA (Layers 00/03/06)

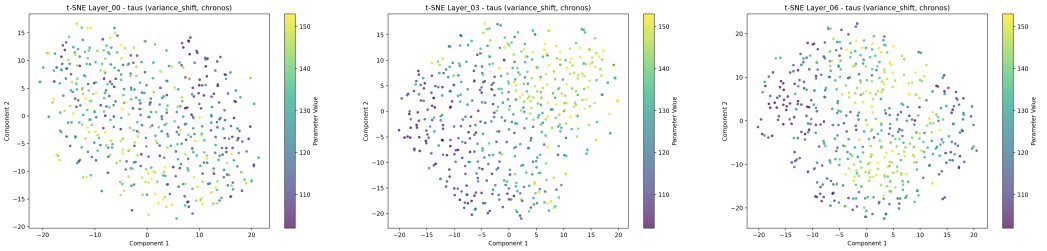

Figure 42: Variance Shift — Chronos — t-SNE (Layers 00/03/06)

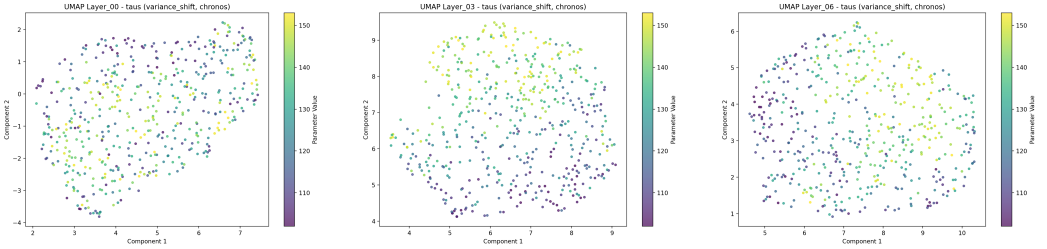

Figure 43: Variance Shift — Chronos — UMAP (Layers 00/03/06)

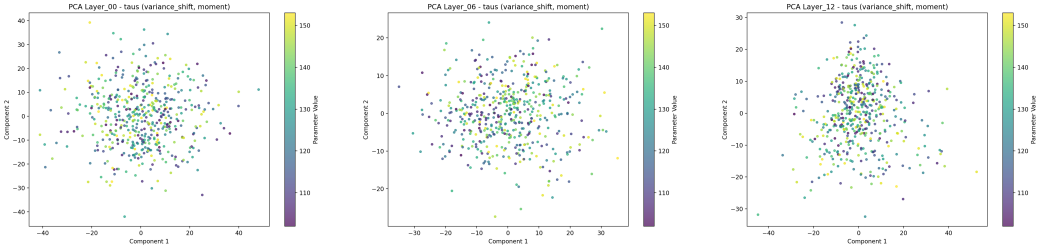

Figure 44: Variance Shift — Moment — PCA (Layers 00/06/12)

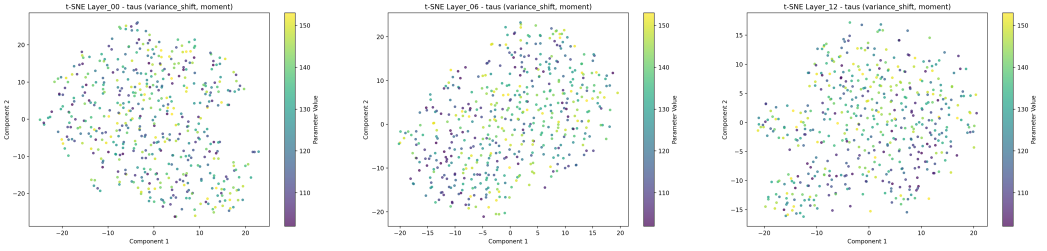

Figure 45: Variance Shift — Moment — t-SNE (Layers 00/06/12)

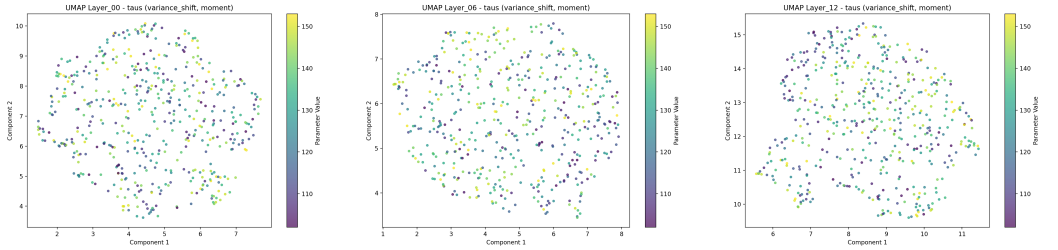

Figure 46: Variance Shift — Moment — UMAP (Layers 00/06/12)

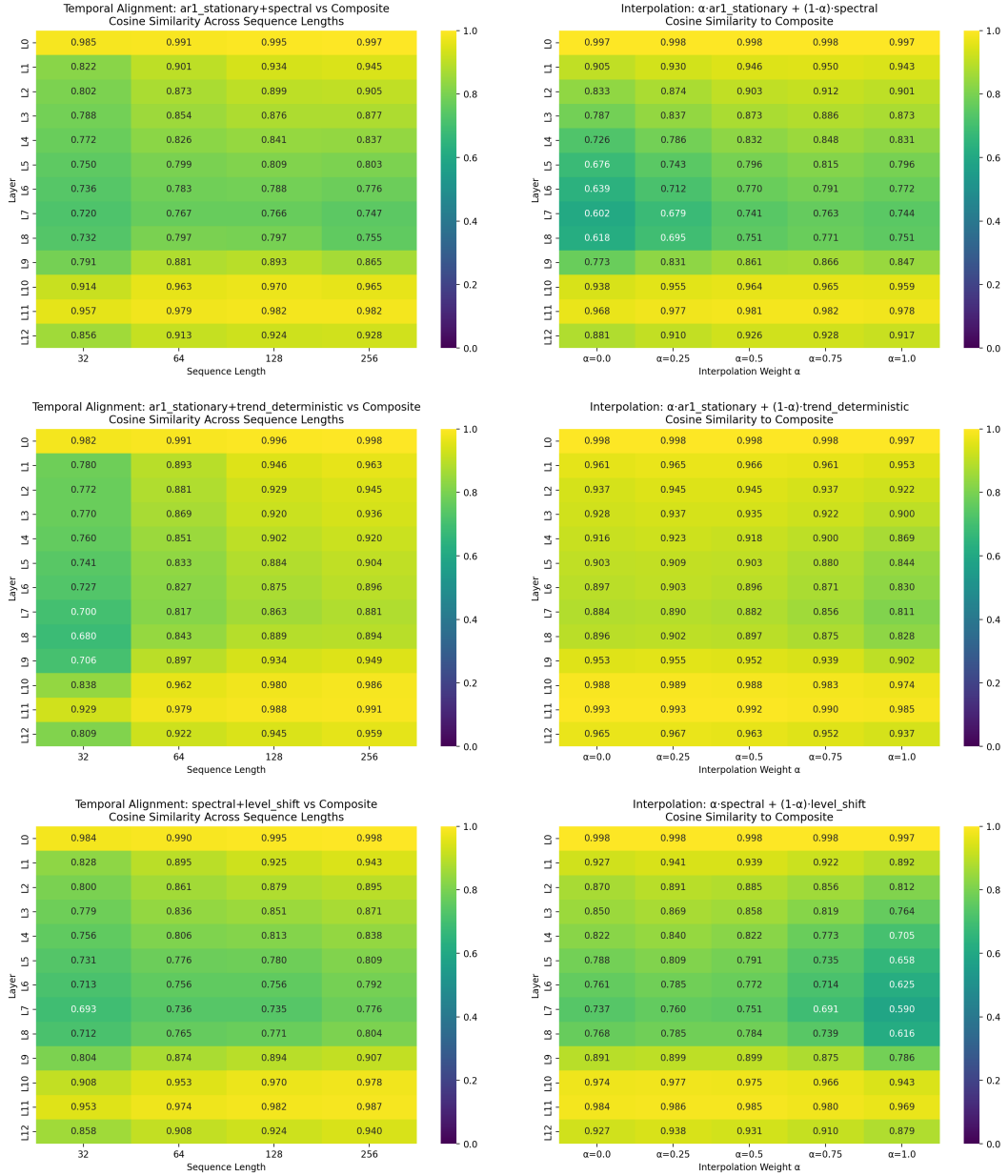

(a) MOMENT - Temporal alignment experiments

(b) MOMENT - Interpolation analysis

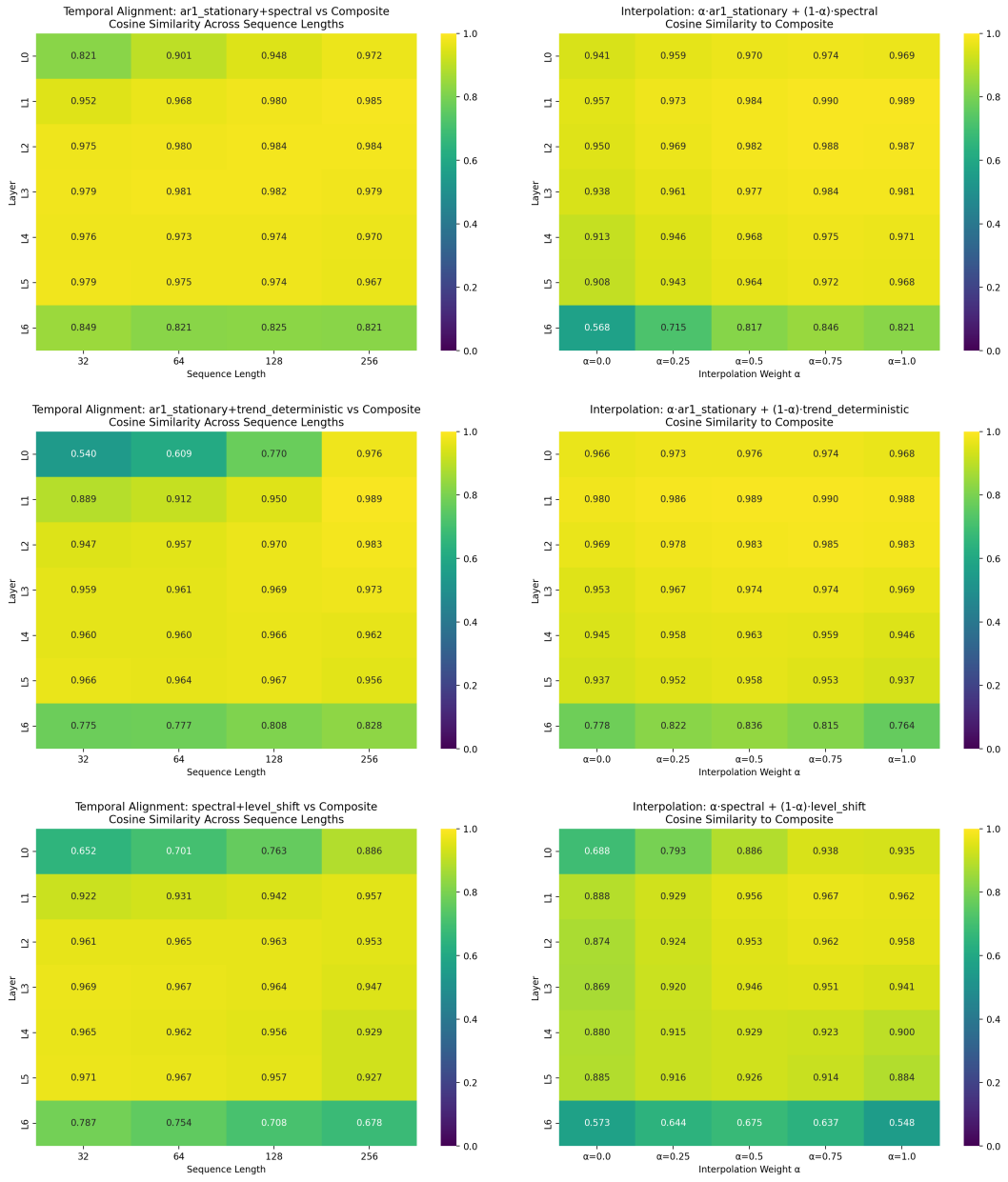

(a) Chronos - Temporal alignment experiments (b) Chronos - Interpolation analysis

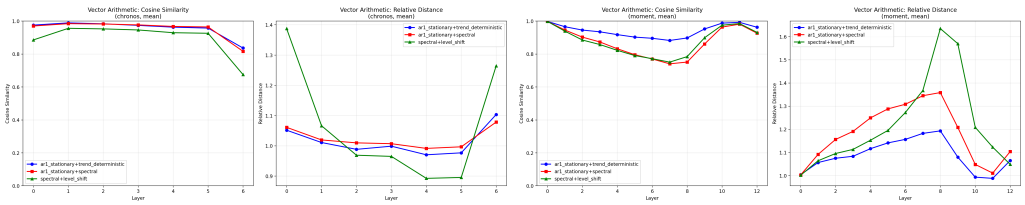

(a) Vector Arithmetic Experiments with Chronos (b) Vector Arithmetic Experiments with MOMENT

Figure 49: Vector Arithmetic Experiments